Investigating controls on boron isotope ratios in shallow marine carbonates

Shuang Zhang [a],[*], Michael J. Henehan [a], Pincelli M. Hull [a], R. Pamela Reid [c], Dalton S. Hardisty [b], Ashleigh v.S. Hood [a], Noah J. Planavsky [a]

[a] *Department of Geology and Geophysics, Yale University, New Haven, CT 06520, USA*
[b] *Woods Hole Oceanographic Institution, Woods Hole, MA 02543-1050, USA*
[c] *Rosenstiel School of Marine and Atmospheric Science, University of Miami, Miami, FL 33158, USA*

A B S T R A C T

The boron isotope-pH proxy has been widely used to reconstruct past ocean pH values. In both planktic foraminifera and corals, species-specific calibrations are required in order to reconstruct absolute values of pH, due to the prevalence of so-called vital effects — physiological modification of the primary environmental signals by the calcifying organisms. Shallow marine abiotic carbonate (e.g. ooids and cements) could conceivably avoid any such calibration requirement, and therefore provide a potentially useful archive for reconstructions in deep (pre-Cenozoic) time. However, shallow marine abiotic carbonates could also be affected by local shifts in pH caused by microbial photosynthesis and respiration, something that has up to now not been fully tested. In this study, we present boron isotope measurements from shallow modern marine carbonates, from the Bahama Bank and Belize to investigate the potential of using shallow water carbonates as pH archives, and to explore the role of microbial processes in driving nominally 'abiogenic' carbonate deposition. For Bahama bank samples, our boron-based pH estimates derived from a range of carbonate types (i.e. ooids, peloids, hardground cements, carbonate mud, stromatolitic micrite and calcified filament micrite) are higher than the estimated modern mean-annual seawater pH values for this region. Furthermore, the majority (73%) of our marine carbonate-based pH estimates fall out of the range of the estimated pre-industrial seawater pH values for this region. In shallow sediment cores, we did not observe a correlation between measured pore water pH and boron-derived pH estimates, suggesting boron isotope variability is a depositional rather than early diagenetic signal. For Belize reef cements, conversely, the pH estimates are lower than likely *in situ* seawater pH at the time of cement formation. This study indicates the potential for complications when using shallow marine non-skeletal carbonates as marine pH archives. In addition, variability in $\delta^{11}B$ based pH estimates provides additional support for the idea that photosynthetic CO_2 uptake plays a significant role in driving carbonate precipitation in a wide range of shallow water carbonates.

© 2016 Elsevier B.V. All rights reserved.

1. Introduction

Determination of ocean pH in the past can provide valuable insights into the geochemical evolution of the ocean and atmosphere. Paleo-pH records can be used to estimate atmospheric CO_2 concentrations (e.g. Foster, 2008), and to help evaluate the relationship between CO_2 concentrations and global climate (e.g. Anagnostou et al., 2016). At present, boron isotope ratios ($\delta^{11}B$) as recorded in marine carbonates are typically thought of as our best means for reconstructing past seawater pH values. The foundation

for the $\delta^{11}B$-pH proxy is a large isotopic fractionation between the two predominant aqueous boron species (trigonal $B(OH)_3$ and tetrahedral $B(OH)_4^-$) and the pH dependence of their relative abundances. Only borate, the charged species, is thought to be incorporated into biogenic carbonates (e.g. Rae et al., 2011), and hence there is a predictable relationship between ocean pH and the $\delta^{11}B$ of $CaCO_3$. This relationship can be summarized by Eq. (1):

$$pH = pK_B^* - \log\left(-\frac{\delta^{11}B_{sol} - \delta^{11}B_c}{\delta^{11}B_{sol} - (^{11-10}K_B \times \delta^{11}B_c) - 1000(^{11-10}K_B - 1)}\right)$$

(1)

where pK_B^* is the dissociation constant for boric acid, $\delta^{11}B_{sol}$ is the isotopic composition of the parent solution, $\delta^{11}B_c$ is the isotopic

---

composition of the carbonate and $^{11-10}K_B$ is the boron isotope fractionation factor between boric acid and the borate ion. $^{11-10}K_B$ has been determined empirically as 1.0272 ± 0.0006 (Klochko et al., 2006) in artificial seawater and later corroborated within uncertainty as 1.026 ± 0.001 (Nir et al., 2015). Although measurements of synthetic calcites to date do not adhere to this theoretical framework (e.g. Noireaux et al., 2015; Sanyal et al., 2000), inorganically precipitated aragonites appear to faithfully record the $\delta^{11}B$ of ambient $B(OH)_4^-$ ion (Noireaux et al., 2015). This suggests that modern aragonitic carbonates should adhere to the theoretical basis of the boron isotope pH proxy laid out in Eq. (1), and therefore could constitute a promising archive for paleo applications.

The boron isotope-pH proxy has been widely applied to foraminiferal calcite to infer past ocean pH and atmospheric CO_2 concentrations over the Cenozoic (e.g. Anagnostou et al., 2016). These applications are supported by the close agreement between boron-derived estimates of atmospheric pCO_2 and values from ice cores (Foster, 2008; Henehan et al., 2013; Hönisch et al., 2009). Importantly, though, these studies rely on the use of appropriate species-specific calibration equations for extant species of foraminifera. Before the evolution of modern foraminiferal species, and when deep sea drill cores are not available, deeper time boron isotope work has focused on shallow marine abiotic carbonates (e.g. micrite from micritic mudsone, dolomicrite and peloids or 'micritized calcispheres'), often targeted to avoid admixture of biogenic material that might have different vital effects (e.g. the Permian–Triassic; Clarkson et al., 2015). However, there are several issues that may cloud reconstruction from micrite. Foremost, micritic mud in the modern day is commonly derived from altered biogenic carbonates, even if this is not visually discernible (e.g. Gischler et al., 2013; Macintyre and Reid, 1995; Reid et al., 1992). This provides the potential for variations in the geochemistry of carbonate mud to primarily reflect the composition of contributing biota, each with their own $\delta^{11}B$ vital effects, rather than variation in the environment. It has also been argued that cyanobacterially-mediated carbonates could be a major source of micrite and peloids (e.g. Berkyová and Munnecke, 2010; Kazmierczak et al., 1996; Pratt, 2001). More broadly, the microenvironment chemistries that produce authigenic abiotic carbonates can be modified by the syntrophic interactions of microbes (e.g. Diaz et al., 2013), raising the potential for disequilibrium in the carbonic acid system relative to surface waters to be predominantly reflected in the geochemistry of these common abiogenic shallow water carbonates. The corollary of this is that B isotopes could provide a novel and potentially very sensitive tool to track microbial influence on shallow water carbonate production, a topic that has been extensively debated (e.g. Diaz et al., 2013; Morse and Mackenzie, 1990).

In this study, we present boron isotope measurements in a wide range of modern shallow marine non-skeletal carbonates from the Bahamas and Belize and compare the back-calculated pH values with local Holocene pH estimates, to test the reliability of using $\delta^{11}B$ in such shallow marine carbonates to infer seawater pH. In the Bahamas, we focused on sediments near the Darby Research Station (Little Darby Island and Lee Stocking Island). Core-top and down-core samples (maximum depth $=\sim 17$ cm) of predominately aragonitic ooids and peloids, core-top oolitic hardground cements, core-top carbonate mud (often called micrite in the geological record despite coarsening during recrystallization) and stromatolitic micrite were collected for analysis. In addition, sediments from a nearby salt pond, red algae (*Neogoniolithon strictum*) from Darby Island and calcified cyanobacteria filament micrite from

Highborne Cay were collected. Finally, botryoidal aragonitic cements from within a Holocene reef limestone from Belize were also analyzed. We discuss the implications of our findings for deep time pH and paleoclimate reconstructions and models of shallow marine carbonate formation.

2. Methods

2.1. Sample selection

Most of our shallow marine carbonates were collected from Little Darby Island and Lee Stocking Island in the Bahamas, close to sampling sites of previous works (Burdige and Zimmerman, 2002; Gischler et al., 2013; Romaniello et al., 2013). Carbonates in this region have been extensively studied and they are often used as a modern analogue for ancient carbonate banks (e.g. Romaniello et al., 2013; Swart et al., 2009). Sediments in this area of the Bahamas are mainly oolite and peloid sands, grapestones and hardgrounds. The dominant mineral phase in local carbonates is aragonite (70–90 wt.%), with high-Mg calcite the second-most-abundant mineral (10–30 wt.%) (Burdige and Zimmerman, 2002; Hu and Burdige, 2007). Radiocarbon dating shows the ooid and peloids shoals across the Bahamas Archipelago have been accumulating for the past 1000–2800 yr (Duguid et al., 2010). Ooids typically have an older inner cortical layer several thousand years old, an outer cortex formed in the last several hundred years and outermost layers formed generally from 200 yr ago to the present (Duguid et al., 2010). Superficial ooids and peloids are abundant outside of active shoals, in part due to extensive micritization of ooids (Reid and Macintyre, 1998).

Sample names and their GPS locations are listed in Table 1 and plotted in Fig. 1. Ooid and peloid sands were measured from eight core-top samples (Cave, Musha, Rudder, Core 1: 0–2 cm, Core 3: 0–2 cm, Core 4: 0–1 cm, Core 6: 0–1 cm and Core 7: 0–1 cm), three down-core samples (Core 1, Core 6 and Core 7) and one salt pond sample (Core 2: 3–5 cm). Core 1 is located in the intertidal zone with a water depth of ~ 1 m during high tide. Core 3 is located within a *Thalassia testudinum* (turtle grass) meadow at a water depth of 2–3 m—this area is proximal to an active ooid shoal but is not currently active due to grass stabilization and is rich in peloids. Cores 4 and 6 were sampled from near Lee Stocking Island, also within a turtle grass bed at a water depth of 7–10 m. Core 7 has no sea grass cover, but was sampled close to Core 4 and Core 6, with a water depth of 7–10 m. The Cave, Musha and Rudder sample sites are all located in the subtidal zone and in active shoals. Core 2 captures the most extreme environment in the sample set, as it was collected from Anaconda Salt pond located in Little Darby Island. Except for Core 1, which gets exposed during low tide, our cores are well below the lowest low tide mark. Hardgrounds were collected in just one sample (a core-top) from Little Darby Island close to Core 3. Carbonate sediments were obtained from Little Darby lagoon, close to where Core 3 was collected. Lagoonal settings such as this are the only facies on the bank top that retain a high portion of fine-grained carbonates, despite extensive production of fine-grained aragonite by benthic green algae in this region. Stromatolites were collected from Lee Stocking Island. Red algae *Neogoniolithon strictum* (composed of high-Mg calcite), were collected from the west side of Darby Island. Thrombolitic microbialites were sampled from Highborne Cay. The calcified filaments in the microbialites transition into micritic cements in the fully lithified samples (Planavsky et al., 2009; Stolz et al., 2009). Finally, we also analyzed two samples of botryoidal cements from a reef slope cavity off Belize (Fig. 2a, b) that had been previously analyzed for $\delta^{13}C$, $\delta^{18}O$ and $\delta^{14}C$ (Ginsburg and James, 1976; Grammer et al., 1993).

Table 1

Bahamas and Belize samples with their GPS location, depth, relevant trace element and boron isotope ratios, derived pH estimates and pore water pH measurements from this study where available. Note in the first column, notations (rep1, rep2, etc.) represent complete replicate analysis of the samples at the same core depth interval (different ooid grain and hardground cement subsamples). The special annotation for Core 7: 0–1 cm (rep1¶ and rep2¶) represents the same sample (after cleaning and dissolution of same ooids grains) passed through columns on separate days and measured on separate days. Annotations for cyanobacterial filaments and red algae (rep1* and rep2*) represents the exact same sample after passing the columns but diluted to different concentrations just before running on the MC-ICP-MS. In the first row, B_{sol} (ppb) represents the boron concentration of the purified post-column boron solution for isotope measurement. Note that all pH estimates are calculated using $^{11-10}K_B$ of 1.0272 ± 0.0006 (Klochko et al., 2006). For red algae, no pH estimates were calculated since they are biotic and are composed of high-Mg calcite instead of aragonite. Core 2: 3–5 cm was also excluded from the calculation, as we have no data for extremes of salinity or major ion chemistry in the salt pond.

Sample name, sample location and sample depth (cm)	B/Ca (µmol/mol)	Mg/Ca (mmol/mol)	Al/Ca (µmol/mol)	B_{sol} (ppb)	$\delta^{11}B$ (‰)	2σ	Calculated pH (total scale)	2σ	Pore water pH (NBS scale)
Cave [23°54′14.40″N, 76°17′50.67″W]									
0–2	216.6	8.8	89.2	49.8	20.95	0.22	8.26	0.05	n/d
Musha [23°53′41.79″N, 76°16′7.65″W]									
0–2	231.9	6.0	74.0	63.4	20.07	0.21	8.19	0.06	n/d
Rudder [23°53′4.67″N, 76°15′36.31″W]									
0–2	191.2	10.3	129.3	41.7	21.09	0.23	8.27	0.06	n/d
Core 1 [23°51′24.59″N, 76°13′30.85″W]									
0–2	261.1	16.4	85.0	50.6	23.24	0.22	8.41	0.05	7.91
2–4	253.2	15.8	80.5	39.2	22.63	0.23	8.37	0.05	7.28
4–6-rep1	231.6	18.9	45.9	32.1	23.72	0.23	8.44	0.05	7.14
4–6-rep2	257.3	23.4	45.5	33.1	23.35	0.23	8.42	0.05	7.14
6–8	246.8	28.0	59.1	39.9	23.65	0.23	8.44	0.05	7.38
8–10	251.2	20.9	63.2	31.3	22.18	0.23	8.34	0.05	7.52
10–12	251.3	20.9	60.0	43.9	23.33	0.23	8.42	0.05	7.78
12–14-rep1	262.7	16.9	62.7	39.0	22.49	0.23	8.36	0.05	7.88
12–14-rep2	301.9	20.9	68.7	16.7	23.00	0.25	8.40	0.05	7.88
Core 2 Salt pond [23°50′51.11″N, 76°12′35.75″W]									
3–5	585.6	17.3	91.7	66.7	25.63	0.21	n/d	n/d	7.39
Core 3 [23°51′24.68″N, 76°13′33.25″W]									
0–2	310.9	36.2	44.3	42.0	24.17	0.23	8.47	0.05	7.67
Core 4 [23°46′11.21″N, 76°6′48.92″W]									
0–1	351.8	43.3	36.3	40.1	23.29	0.23	8.42	0.05	n/d
Core 6 [23°46′11.21″N, 76°6′48.92″W]									
0–1-rep1	235.5	18.0	104.3	24.3	20.82	0.24	8.25	0.06	7.72
0–1-rep2	260.1	19.2	46.5	58.8	21.52	0.22	8.30	0.06	7.72
3–5	271.5	16.2	50.3	39.3	21.41	0.23	8.29	0.06	7.56
5–7-rep1	232.9	19.2	58.6	66.6	21.77	0.22	8.31	0.05	7.56
5–7-rep2	255.9	31.2	66.0	23.8	21.97	0.24	8.33	0.05	7.56
5–7-rep3	242.5	18.4	46.1	27.4	21.40	0.24	8.29	0.05	7.56
7–9-rep1	239.2	22.0	62.1	65.3	21.90	0.21	8.32	0.05	n/d
7–9-rep2	254.9	17.4	115.9	41.2	21.15	0.23	8.27	0.06	n/d
7–9-rep3	232.6	14.2	31.8	56.4	20.13	0.22	8.19	0.06	n/d
9–11-rep1	279.1	20.5	74.8	26.9	21.39	0.24	8.29	0.05	7.46
9–11-rep2	245.5	19.8	81.9	32.8	22.33	0.23	8.35	0.05	7.46
11–13-rep1	285.3	29.4	137.4	23.6	22.45	0.24	8.36	0.05	7.44
11–13-rep2	246.6	10.7	41.7	42.9	20.55	0.23	8.23	0.06	7.44
13–15-rep1	293.5	37.0	106.9	29.1	22.51	0.24	8.36	0.05	n/d
13–15-rep2	313.7	18.4	85.9	28.2	21.89	0.23	8.32	0.05	n/d
15–17	264.7	28.7	71.6	64.7	22.39	0.22	8.36	0.05	7.31
Core 7 [23°46′10.78″N, 76°6′51.48″W]									
0–1-rep¶	254.6	16.3	45.6	60.7	21.60	0.21	8.30	0.05	n/d
0–1-rep2¶	254.6	16.3	45.6	44.1	21.54	0.23	8.30	0.05	n/d
0–1-rep3	290.5	12.5	75.6	36.4	20.56	0.23	8.23	0.06	n/d
0–1-rep4	259.6	15.5	53.4	40.8	21.64	0.23	8.30	0.05	n/d
0–1-rep5	260.0	13.7	52.0	50.2	21.33	0.23	8.28	0.06	n/d
0–1-rep6	252.4	16.0	41.3	65.0	20.16	0.21	8.20	0.06	n/d
1–2	232.9	8.1	32.3	75.5	20.06	0.21	8.19	0.06	n/d
2–3	228.2	9.7	50.2	45.4	20.23	0.22	8.20	0.06	n/d
3–4	225.4	9.2	48.1	61.9	19.70	0.21	8.16	0.06	n/d
6–7	254.7	17.5	52.5	68.8	21.15	0.20	8.27	0.06	n/d
Hardground cement [23°51′22.13″N, 76°13′41.52″W]									
rep1	336.0	44.3	73.2	28.1	22.99	0.23	8.40	0.05	n/d
rep2	321.5	45.3	91.7	35.4	22.83	0.23	8.39	0.05	n/d
Cyanobacterial filament micrite [24°43′0.00″N, 76°48′60.00″W]									
rep1*	651.6	14.9	49.9	52.7	25.58	0.22	8.56	0.05	n/d
rep2*	651.6	14.9	49.9	30.9	25.57	0.23	8.56	0.05	n/d
Carbonate mud (near Core 3)									
Carbonate mud #1	n/d	n/d	n/d	16.4	22.70	0.24	8.38	0.05	n/d
Carbonate mud #2	n/d	n/d	n/d	18.3	23.02	0.23	8.40	0.05	n/d
Carbonate mud #3	n/d	n/d	n/d	36.3	22.55	0.22	8.37	0.05	n/d
Stromatolitic micrite (near Core 7)									
Stromatolitic micrite	n/d	n/d	n/d	20.3	22.07	0.23	8.33	0.05	n/d
Red algae [23°50′21.54″N, 76°13′12.52″W]									
rep1*	716.3	285.1	60.2	54.2	32.42	0.22	n/d	n/d	n/d
rep2*	716.3	285.1	60.2	22.9	32.63	0.24	n/d	n/d	n/d
Belize cement [16.7°N, 87.5°W]									
#1	317.7	9.8	127.8	5.8	17.70	0.68	7.98	0.08	n/d
#2	225.2	6.4	57.3	28.9	17.65	0.23	7.97	0.06	n/d
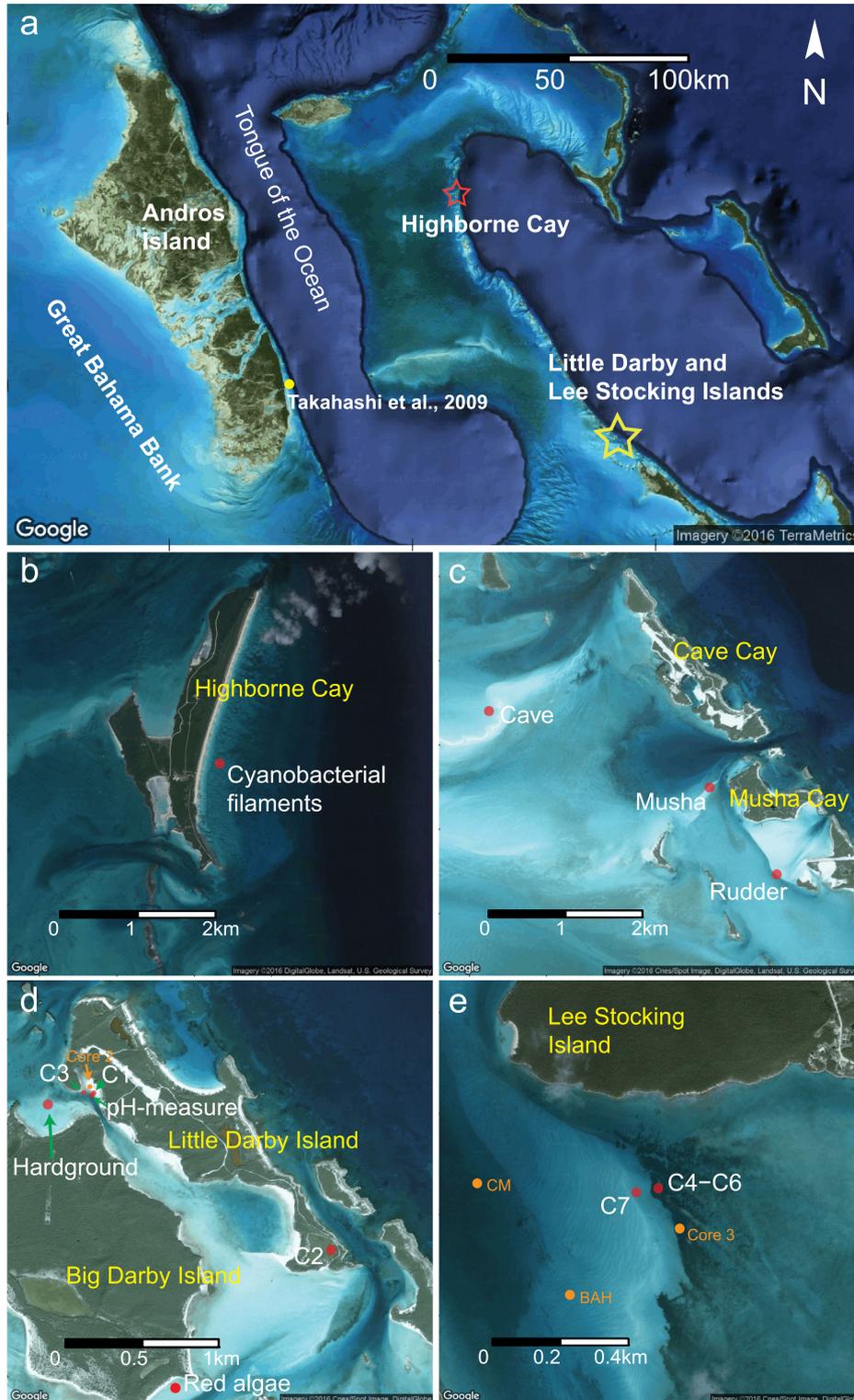
Fig. 1. Site locations in the Bahamas (see Table 1 for further details). (a) Map of the study area. Yellow filled circle shows the grid point used for temperature, salinity, and air–sea CO_2 disequilibrium parameters (Takahashi et al., 2009). (b) Calcified cyanobacterial filaments sample location in Highborne Cay. (c) Ooid collection locations from Cave Cay and Musha Cay north of Little Darby Island. (d) Ooid, hardground and red algae collection locations from Little Darby Island and Big Darby Island. Location of one-day long tidal cycle pH measurements also indicated. (e) Ooid collection locations from Lee Stocking Island. Also shown is the sampling locations of other studies including CM: Burdige and Zimmerman (2002), BAH: Gischler et al. (2013), and Core 2 and Core 3: Romaniello et al. (2013). Note that Belize cements were not plotted in this figure. Their location is described in Ginsburg and James (2013) and Grammer et al. (1993). (For interpretation of the references to color in this figure legend, the reader is referred to the web version of this article.)
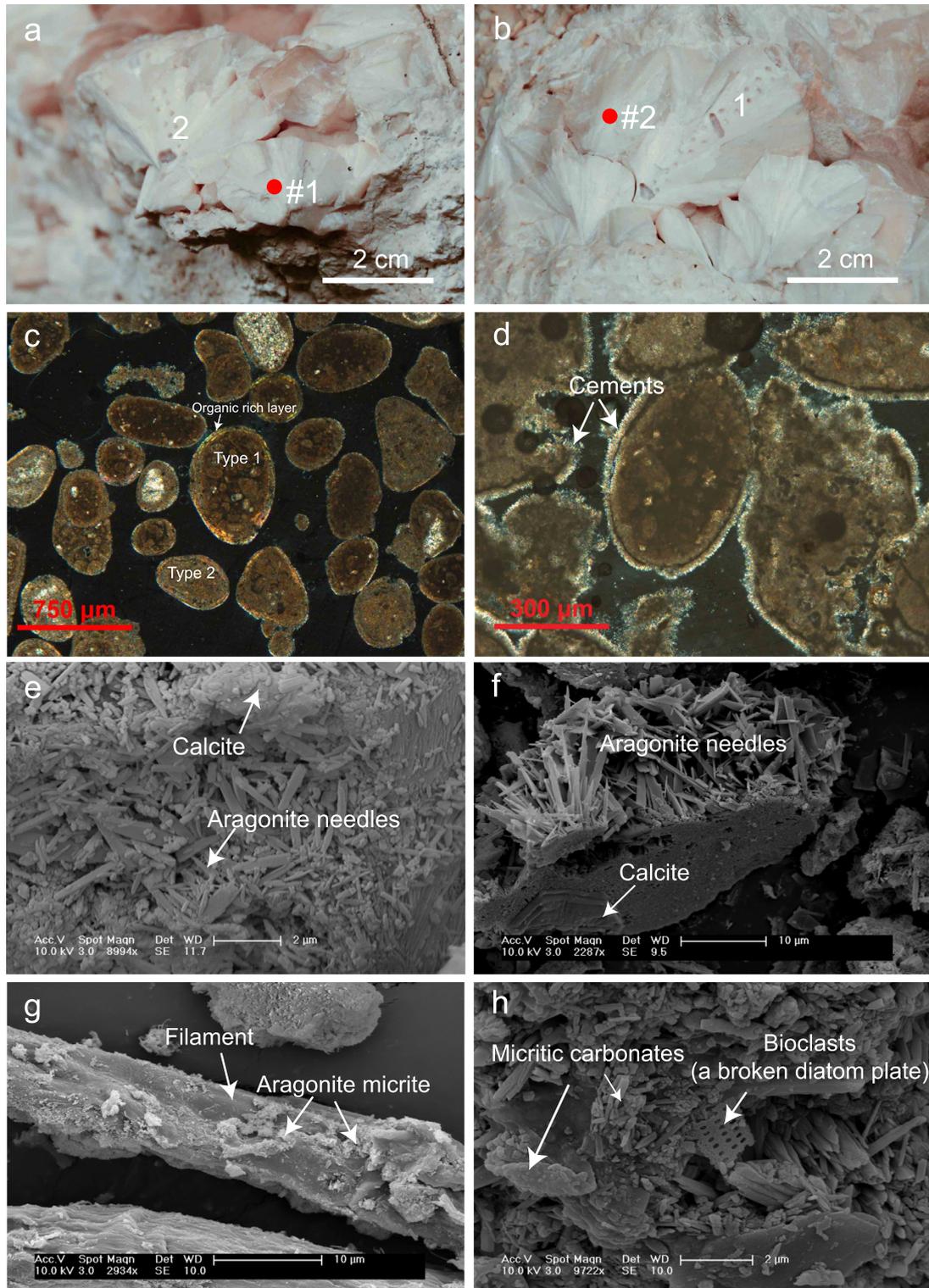
Fig. 2. Photos of our Bahamas and Belize samples. (a), (b) Photos of the Belize aragonite cement fans. The areas previously analyzed for δ^{13}C, δ^{18}O and δ^{14}C (Ginsburg and James, 1976; Grammer et al., 1993) are denoted as 2 and 1. Our sampling areas are marked by the red dots and denoted as #1 and #2. (c) Thin section of Musha under polarized light. The shiny outer layers of the ooids represent aragonite needles and the darker interlayers indicate a high organic content. Two types of nuclei were detected. The first one is composed of random material (e.g. pellets, peloids, occasionally bioclastics and even smaller ooids) and the second one is a micritic ellipsoidal chunk. (d) Thin section of hardground under the polarized light. The grains are cemented by an irregular mesh of aragonite needles and laths. (e) SEM image of Core 6: 0–1 cm. Aragonite needles are widespread on the ooids surface. Calcite overgrowths are also observed on the ooids surface. (f) SEM image of separated cements from hardground. The cements are composed of clusters of aragonite needles, along with sporadic calcite. (g) SEM image of separated calcified filaments. Clusters of aragonitic micrite surrounded the cell. (h) SEM image of separated carbonate mud from Little Darby lagoon. Individual and clustered micritic crystals dominate, with occasional bioclasts. (For interpretation of the references to color in this figure legend, the reader is referred to the web version of this article.)

2.2. pH analysis

All local pH measurements were conducted in the Darby Island Research Center. The pH electrode was calibrated using three NIST (National Institute of Standards and Technology) pH buffers (i.e. 4.01, 7.00, and 10.01), thus producing pH values on the NBS (National Bureau of Standards) scale. Surface water pH at Little Darby Island (as shown in Fig. 1d) was measured every 1 or 2 h over the course of a whole day on December 24th, 2015. For some samples (Core 1, Core 2, Core 3 and Core 6), pore water pH was measured immediately after collection, using rhizons for pore water extraction. Given that we are sampling sites that are flushed by open ocean waters (to the east of the Bahama Bank) and that $\delta^{11}B$ of seawater ($\delta^{11}B_{SW}$) is globally homogeneous (Foster et al., 2010), we did not sample bank waters to measure the was $\delta^{11}B_{SW}$.

2.3. Carbonate analysis

2.3.1. Solid characterization

X-ray diffraction (XRD) analyses were conducted on powdered bulk ooid sand samples (Core 1, Core 3, Core 4, Core 6 and Core 7) in the XRD lab of the University of Miami using a Scintag XDS 2000 (Swart et al., 2002). The 2σ uncertainty on mineral proportions determined by XRD analysis is ± 2 wt.%. Scanning electron microscope (SEM) analysis conducted at Department of Geology and Geophysics at Yale University. Several sediment samples and one hardground sample were cast in resin, from which thin sections were prepared. Photographs were taken on a standard petrographic microscope under plain and polarized light.

2.3.2. Sample preparation for trace elements and boron isotope analysis

Hardgrounds were first gently broken into powders and chunks. Afterwards, the fine powders were passed through a 32 µm sieve to separate the fine cement sample from other larger sand grains and bioclasts. The stromatolitic micrite (< 32 µm) were collected in the same way as hardground cements. Little Darby lagoon sediment samples were also passed through a 32 µm sieve to separate the carbonate mud from other sand grains and bioclasts. Cavity-filling, botryoidal aragonite cements (of up to 4 cm in crust thickness) were microdrilled with a diamond drill bit to obtain powders for analysis. Calcified cyanobacterial filaments were torn apart using tweezers and passed through a 90 µm sieve to separate the calcified filament sample material from hard sand grains. Ooids were picked individually from each sediment sample to avoid contamination from bioclasts, shell fragments and oxides. After preparation, all laboratory procedures were carried out in a Picotrace clean lab inside an overpressured hood equipped with boron-free filters. In this way, contamination from airborne boron during sample preparation was minimized, with fall-in blank in the overpressured hood of 0.21 pg/h.

Approximately 1 mg of solid carbonate was cleaned following procedures described in Rae et al. (2011) and Henehan et al. (2013). The solid was ultrasonicated and rinsed repeatedly using Milli-Q water (18.2 MΩ, with Q-Gard boron removal pack) to remove clays and any contaminants from handling. Afterwards, to remove the organic content, the solid was subjected to oxidative cleaning (using 250 µL 1% H_2O_2 in 0.1 M NH_4OH at 80 °C) lasting 15 min in total (3×5 min, with 15 s ultrasonication in between). Following this, 0.0005 M HNO_3 was added to the sample for a brief weak acid leach to remove any re-adsorbed contaminants. Subsequently, 200 µL Milli-Q water was added to each sample and 0.5 M HNO_3 was added incrementally until the sample was totally dissolved. Finally, the sample was centrifuged for ~5 min in order to isolate any undissolved contaminant phases. 20 µL of supernatant was transferred to an acid-cleaned plastic centrifuge tube for trace element analysis. The remaining supernatant was transferred to a Teflon beaker for isotope analysis.

Prior to MC-ICP-MS analysis, boron was separated from the dissolved carbonate matrix by passing through pre-cleaned heat-shrunk Teflon columns containing 20 µl of ground, sieved (63–100 µm) boron-specific anionic exchange resin Amberlite IRA 743 (Kiss, 1988), following Foster (2008). Boron-clean Na acetate-Acetic acid buffer was added to samples prior to column chemistry to maintain sample pH > 5. Matrix was the rinsed through by addition of 10×160 µl Milli-Q, before sample was eluted in 5×120 µl 0.5 M HNO_3. An additional 120 µl elution step was monitored to ensure complete sample elution. Each batch of columns included a JCp-1 carbonate geostandard (Japanese Geological Survey Porites Coral, Okai et al., 2002) to monitor column behavior and reproducibility, and a total procedural blank (TPB; comprised of 0.5 M HNO_3 and buffer) to monitor cleanliness, and potential of sample contamination.

2.3.3. Trace element analysis by ICP-MS

Trace element concentrations were analyzed on a Thermo Element XR ICP-MS at the Yale Metal Geochemistry Centre (YMGC) using a Teflon barrel spray chamber and ammonia gas to improve boron washout, following Rae et al. (2011). In-house consistency standards were analyzed to monitor machine behavior. To optimize reproducibility, sample matrix was matched to the [Ca] of bracketing standards and analyzed for a full trace metal suite (i.e. Li, B, Na, Mg, Al, Mn, Sr, Ba, Nd, U). Long-term reproducibility of the measurements as determined by repeat analysis of in-house standards is typically better than 5% (2σ uncertainty).

2.3.4. Boron isotopic analysis by MC-ICP-MS

Boron isotope analyses were performed on Thermo Neptune Plus MC-ICP-MS equipped with 10^{12} Ω resistors at the YMGC following the procedure of Foster (2008). As with trace element analysis, a Teflon barrel spray chamber was used, with ammonia gas added to improve washout. Samples were bracketed with 50 ppb NIST SRM 951 boric acid standard, measured in duplicate and the mean $\delta^{11}B$ reported. The blank contribution from total procedural blanks (TPBs) was ~52 pg on average (~0.17% of the average sample size). TPBs were measured and used to correct sample $\delta^{11}B$ values. The average size of the blank correction ($\delta^{11}B_{original} - \delta^{11}B_{corrected}$) is < 0.1‰, and therefore typically below measurement uncertainty. The uncertainty of boron isotope measurements was determined from a relationship (Eq. (2) below) between signal size and external reproducibility:

$$2\sigma = 8.67 \times \exp\left(-42.21\left[^{11}B\right]\right) + 0.25 \times \exp\left(-0.21\left[^{11}B\right]\right) \quad (2)$$

where $[^{11}B]$ is the intensity of ^{11}B signal in volts. This is derived from repeat analysis of multiple batches of roughly mass-matched JCp-1, cleaned and dissolved, and passed through columns with individual sample batches (see Table S1). For sample sizes comparable to the typical carbonate samples in this study ($> \sim 13$ ngB), the average $\delta^{11}B$ value of JCp-1 is 24.22 ± 0.20‰ (2σ, $n = 10$). Laboratory accuracy is further demonstrated by measurements of ERM boric acid standards AE120 (certified value $= -20.2 \pm 0.6$‰; 2σ) and AE121 (certified value $= 19.9 \pm 0.6$‰; 2σ) (Vogl and Rosner, 2012). Our measured values for these standards are given in Table S2 and S3, with a mean value for AE120 of -20.27 ± 0.23‰ (2σ, $n = 15$) and a mean value for AE121 of 19.54 ± 0.15‰ (2σ, $n = 16$). As a further test of intermediate reproducibility, one sample, the Core 7: 0–1 cm sample (after cleaning and dissolution) was passed through columns on separate days and measured on separate days, and yielded values of 21.60‰ and 21.54‰, demonstrating the reproducibility of our analyses for real samples.

2.3.5. C–O isotope analysis

Carbon and oxygen isotope ratios of our carbonate samples (picked ooids and sieved sediments) were measured at the Yale Analytical and Stable Isotope Center (YASIC) on a Thermo Kiel IV online carbonate preparation device coupled to a MAT 253 mass spectrometer and are reported relative to VPDB. External analytical precision (2σ) is 0.06‰ for $\delta^{13}C$ and 0.07‰ for $\delta^{18}O$ based on replicate analyses of in-house (PX, TS) and international (NBS19) standards.

2.4. Hydrographic data

Most of the hydrographic data used in this study are taken from the gridded dataset of Takahashi et al. (2009). Intra-annual variations in hydrographic parameters (e.g. sea surface temperature, salinity, alkalinity, pre-industrial pH values, modern pH values and Belize pH values) are listed in Table S4. The microelectrode pH measurements (in NBS scale) near Little Darby Island mentioned above were converted to total scale, as listed in Table S5. For details on calculation procedures and the derivation of these pH values, see Supp. Text.

2.5. pH estimates from boron isotopes

Back-calculation of pH from boron isotopes was conducted for our abiotic aragonitic samples (i.e. ooids, hardground cements, cyanobacterial filament micrite, lagoonal micritic sediments, stromatolite micrite and Belize cements) but not for red algae since vital effects for coralline algal carbonates are poorly quantified. Core 2: 3–5 cm was also excluded from the calculation, as we have no data for extremes of salinity or major ion chemistry in the salt pond. For full details of calculation procedures, see Supp. Text. Briefly, we assume a $^{11-10}K_B$ of 1.0272 ± 0.0006 (2σ) from (Klochko et al., 2006). Calculations using a $^{11-10}K_B$ of 1.026 (Nir et al., 2015) are given in Table S6. pK_B^* was calculated as 8.567 ± 0.043 (2σ) from nearby estimates of mean annual temperature ($26.93\,°C$) and salinity (36.43), with uncertainty on this parameter reflecting intra-annual variability. All calculations assume a $\delta^{11}B_{sw}$ of 39.61 ± 0.04‰ (Foster et al., 2010).

3. Results

3.1. Pore water pH characteristics

Available pore water pH values for different cores are listed in Table 1. All the pore water pH values (7.14–7.91, NBS scale) are lower than our microelectrode pH measurements of surface pH in this area (8.04–8.19, NBS scale), and also lower than either modern (8.16–8.20, NBS scale) or pre-industrial (8.27–8.33, NBS scale) pH values calculated from the nearby Takahashi et al. (2009) grid point. Pore water pH profiles are shown in Fig. 4. For Core 1, pore water pH decreased by 0.77 units from 7.91 to 7.14 at 5–6 cm depth, before gradually increasing to 7.88 by 13 cm depth. For Core 6, pH decreases more uniformly from 7.72 close to the surface down to 7.31 at 15–17 cm depth. The pH profile of Core 1 is similar to that observed in sediments without turtle grass from Lee Stocking Island by Burdige and Zimmerman (2002), while pH in Core 6, below dense turtle grass, also resembles a nearby pore water pH profile measured within a turtle grass colony by these authors.

3.2. Carbonate characteristics and mineralogy

Ooids examined in this study typically displayed a large nucleus and a very thin concentric cortex (multiple concentric layers) based on thin section petrography (Fig. 2c). The polished outer layers of the ooids are composed of aragonite needles, which are interlaminated with darker layers, indicating a higher organic content. Microbe borings are present as small, brown-dark circular and linear features cross cutting ooid laminae, which are more evident under SEM (Fig. S1a, b). Ooids display two types of nuclei. The first nucleus type (Fig. 2c, Type 1) consists of random grains (e.g. pellets, peloids, bioclasts, and even smaller ooids), which were probably detrital grains rolled by waves and currents, to accumulate ooid coatings. Based on grain counts in thin sections, bioclasts in the picked ooids and peloids were estimated to represent less than 4% of grain nuclei. The dominant type of nucleus (Fig. 2c, Type 2) is entirely micritic, possibly originating as micrite peloids, or as grains that were micritized on the seafloor prior to the formation of ooid laminae. Both aragonite needle cements and occasional encrusting calcite overgrowths are observed on the ooid surfaces with SEM (Fig. 2e). Hardground fragments consist of a variety of grains that are isopachously cemented by an irregular mesh of aragonite needles and laths (Fig. 2d) similar to those described by Ginsburg and Planavsky (2008). The cements separated for measurement are composed largely of clusters of aragonite needles, along with minor amounts of calcite (Fig. 2f). Separated calcified filaments from the thrombolitic microbialites show micritic aragonite surrounding the cell (Fig. 2g). Carbonate mud from Little Darby lagoon is mainly composed of micritic carbonate clusters, along with occasional bioclasts (Fig. 2h). Stromatolitic micrite is mainly composed of aragonite (Fig. S1c). SEM observations of Belize reef cements (Fig. S1d) confirm the acicular aragonite texture described by Ginsburg and James (1976).

XRD analyses (Table S7) show that aragonite is the main component of the bulk core samples, with an average value of 85 wt.% ($2\sigma = 15\%$). The average values of high-Mg calcite and low-Mg calcite are 14 wt.% ($2\sigma = 13\%$) and 1 wt.% ($2\sigma = 3\%$), respectively. Similar carbonate composition values for sediments in the Bahamas have also been observed in other studies (Hu and Burdige, 2007; Morse et al., 1985), although cores from this study display considerable variation in carbonate composition. For instance, although collected from the same site, the proportion of aragonite in Core 4: 0–1 cm sediments is 78.3%, which is 11% more than that of Core 6: 0–1 cm, with 67.0% aragonite. The average proportion of aragonite for all samples from Core 6 is 81.3%, which is 11% less than average values of 92.9% in Core 7, even though the two cores are only ∼ 80 m apart. These results demonstrate that carbonate composition in this study area is heterogeneous, even on small spatial scales. We note that in the geologic record, these sediments would likely be recorded as calcite peloids and ooids due to early burial phase diagenesis, assuming no later stage dolomitization (Morse and Mackenzie, 1990).

3.3. Trace element ratios in carbonates

For most samples, B/Ca ratios are in the range of 200–350 µmol/mol (Table 1). Several exceptions exist. Core 2: 3–5 cm, from a high salinity pond, displays a high B/Ca ratio of 586 µmol/mol. Calcified cyanobacterial filaments and red algae also show high B/Ca ratios of 651 and 716 µmol/mol, respectively. Similarly high B/Ca ratios in one red algae sample (*Goniolithon*, 695 µmol/mol) were observed by Hemming and Hanson (1992). The B/Ca ratios in our samples are typical of aragonite and high-Mg calcite (Hemming et al., 1995; Noireaux et al., 2015). An additional observation of note is the large difference (∼100 µmol/mol) in B/Ca ratios in core-tops from Cores 4 (352 µmol/mol) and 6 (248 µmol/mol), which again highlights the relatively large heterogeneity among predominantly aragonitic ooids even in the same location. Variation in Mg/Ca ra-

tios is also observed within and among cores. All trace elements (i.e. Li, B, Na, Mg, Al, Mn, Sr, Cd, Ba, Nd, U) are listed in Table S8. All of the samples presented here have Al/Ca ratios lower than 140 μmol/mol (Table 1) indicating little or no contamination from clay-adsorbed boron.

3.4. C–O isotope signatures

Carbon and oxygen isotope ratios (in VPDB scale) for the Bahamas ooids (excepting core 2) are in the normal range of typical shallow marine abiotic carbonates. $\delta^{13}C$ ranges from 4.27 to 5.26‰ and $\delta^{18}O$ ranges from -0.48 to 0.24‰, which are in agreement with published values of modern shallow-water Bahamas carbonate sediments (e.g. Lowenstam and Epstein, 1957; Swart et al., 2009). The hardground cements ($\delta^{13}C$ is 3.81‰ and $\delta^{18}O$ is -0.65‰) are also in the same range of typical marine cement (Grammer et al., 1993). The carbonate mud sieved from the lagoonal sediments show a wider range of C–O isotopes, with $\delta^{13}C$ ranging from 1.85 to 3.04‰ and $\delta^{18}O$ ranging from -1.47 to -0.59‰. The red algae display the lowest $\delta^{13}C$ (-1.27‰) and $\delta^{18}O$ (-4.74). For Belize cements, $\delta^{13}C$ ranges from 0.76 to 0.92‰ and $\delta^{18}O$ ranges from 4.24 to 4.35‰, which is within the range of previous studies: $\delta^{13}C$ from 0.60 to 2.07‰ and $\delta^{18}O$ from 3.52 to 4.86‰ (Grammer et al., 1993).

3.5. Boron isotope signatures and pH estimates

There are large variations in $\delta^{11}B$ between different types of carbonates examined, different cores, different depths within each core and even among the different duplicate ooids samples picked from the same depth interval in the same core (Table 1 and Fig. 3a). Belize cements display the lowest $\delta^{11}B$ (17.68‰) and red algae show the highest $\delta^{11}B$ (32.52‰). For abiotic aragonitic ooids, peloids, hardground cements, calcified aragonitic filaments, carbonate mud and stromatolitic micrite in the Bahamas, $\delta^{11}B$ ranges from 19.70‰ to 25.63‰, with an average of 22.12‰ ($2\sigma = 2.82$). This range is comparable to the variation in $\delta^{11}B$ of planktic foraminifera (11.54‰ to 20.34‰) reported across the entire Eocene (Anagnostou et al., 2016). No coherent pattern can be observed in the change of $\delta^{11}B$ with depth for each core (Table 1 and Figs. 3a).

The *in situ* pH inferred from $\delta^{11}B$ measurements is plotted for each sample in Fig. 3b. As expected from the large variability in $\delta^{11}B$, large variations in pH estimates exist between different samples. For Bahamas samples, pH estimates derived from core-top samples, surface hardground cements and microbial carbonates (8.19–8.56) show a large variance and do not match either estimated modern seawater pH values for this region (8.04, $2\sigma = 0.04$) or our pH measurements from this area (7.99, $2\sigma = 0.10$). The majority of our pH estimates also fall outside of the range of estimated pre-industrial seawater pH values ($\sim$8.16, $2\sigma = 0.06$). pH derived from down-core samples (8.16–8.44) shows a similarly large variance both within the same core and between cores. pH estimates from boron isotopes do not show a constant offset from seawater pH values, nor is there a statistically discernible relationship (R-squared $= 0.04$, $p = 0.43$) with pore water pH in either Core 1 or Core 6 (Fig. 4). For Belize cements, back-calculated pH estimates ($\sim$7.98) are lower than seawater pH ($\sim$8.17) estimated for this region 11 kyr to 12 kyr ago. For the Bahamas samples, calculating pH using the fractionation factor from Nir et al. (2015) as in Table S6, brings the pH estimates from carbonates closer to seawater pH values. However, the majority of pH estimates are still higher than seawater pH values and large variations exist among calculated pH.

4. Discussion

4.1. Comparison with published $\delta^{11}B$ values in inorganic carbonates

Boron isotope and B/Ca ratios in the ooids presented here are in approximate agreement with previous measurements of marine ooids from the Bahamas, and the Turks and Caicos Islands (21.2‰–22.2‰ and 227–261 μmol/mol; Hemming and Hanson, 1992). To better consider our non-skeletal carbonate observations (ooids, cements and filaments) in the context of published patterns of $\delta^{11}B$ variation in inorganic precipitates (Hemming et al., 1995; Hemming and Hanson, 1992; Noireaux et al., 2015; Sanyal et al., 2000), these data are plotted together in Fig. 5. While it is clear from Fig. 5 that $\delta^{11}B$ values in experimentally-precipitated calcites from non-natural seawater vary considerably from the $\delta^{11}B$ of aqueous borate ion, aragonite precipitates from Noireaux et al. (2015) display absolute values and a pH-sensitivity within uncertainty of that expected from aqueous borate (and in exact agreement if a value of $^{11-10}K_B$ of 1.026 ± 0.001 is assumed; see Fig. S2). Therefore, observations from inorganic precipitation studies would suggest that our predominantly aragonitic ooids should, barring other compounding factors, reflect the $\delta^{11}B$ values of borate ion. As is evident in Fig. 5, this is not the case: the majority of our data from aragonitic samples fall well above the 1:1 line. Further, the offset from $\delta^{11}B_{borate}$ is not constant across different samples (from 0 offset to 5.88‰ offset) at the same seawater pH.

4.2. Causes of the $\delta^{11}B$ variation in shallow modern marine carbonates

There has been extensive debate for decades over the origin of ooids (or more precisely, ooid cortex formation) and the potential contribution of microbial processes to 'abiogenic' carbonate formation more broadly (e.g. Diaz et al., 2013; Morse and Mackenzie, 1990). Traditionally most workers favored a primarily abiotic model of ooid formation (e.g. Davies et al., 1978; Land et al., 1979), based largely on ooid morphology, crystal structure and isotope analysis. However, organic coatings (generated by microbes) may provide nucleation sites for carbonate precipitation and the microbial communities present in shallow marine sediments may also alter local carbonate chemistry during and after ooid cortex formation. Recent evidence for diverse microbial communities within modern ooids, including photosynthetizers, provides additional support for such an influence of microbial activity on ooid cortex formation (e.g. Diaz et al., 2013; Summons et al., 2013).

If the Bahamian aragonitic ooids were truly abiotic precipitates, based on the results of Noireaux et al. (2015), they should have a $\delta^{11}B$ close to the borate ion values of seawater. To explain these deviations through hydrographic conditions at the moment of precipitation (i.e. extreme values of pK_B^* at the time of precipitation), sea water temperatures of $>60\,^\circ$C would be required in some cases. Since this is unfeasible, we suggest that anomalous temperature and salinity cannot explain the variations in $\delta^{11}B$ values of ooids reported in this study. Instead, microbial influence (e.g. photosynthesis; Diaz et al., 2013) on ooid and peloid formation and/or later-stage microbial (marine) diagenetic alteration of ooids (Reid and Macintyre, 2000), could readily lead to a large range of microenvironment pH, and hence $\delta^{11}B$ values, similar to what we observe. The abundance of organic layers and widespread microborings (Fig. 2c and Fig. S1a, b) in our ooid cortices suggest an intimate association of ooids and microbes. The majority of $\delta^{11}B$ values are higher than that of the borate ion in seawater (Fig. 5), suggesting ooid formation in an environment with elevated pH, relative to seawater. Photosynthetic CO_2 uptake (potentially by endolithic cyanobacteria) is the most likely mechanism to drive a pH rise and facilitate carbonate precipitation in
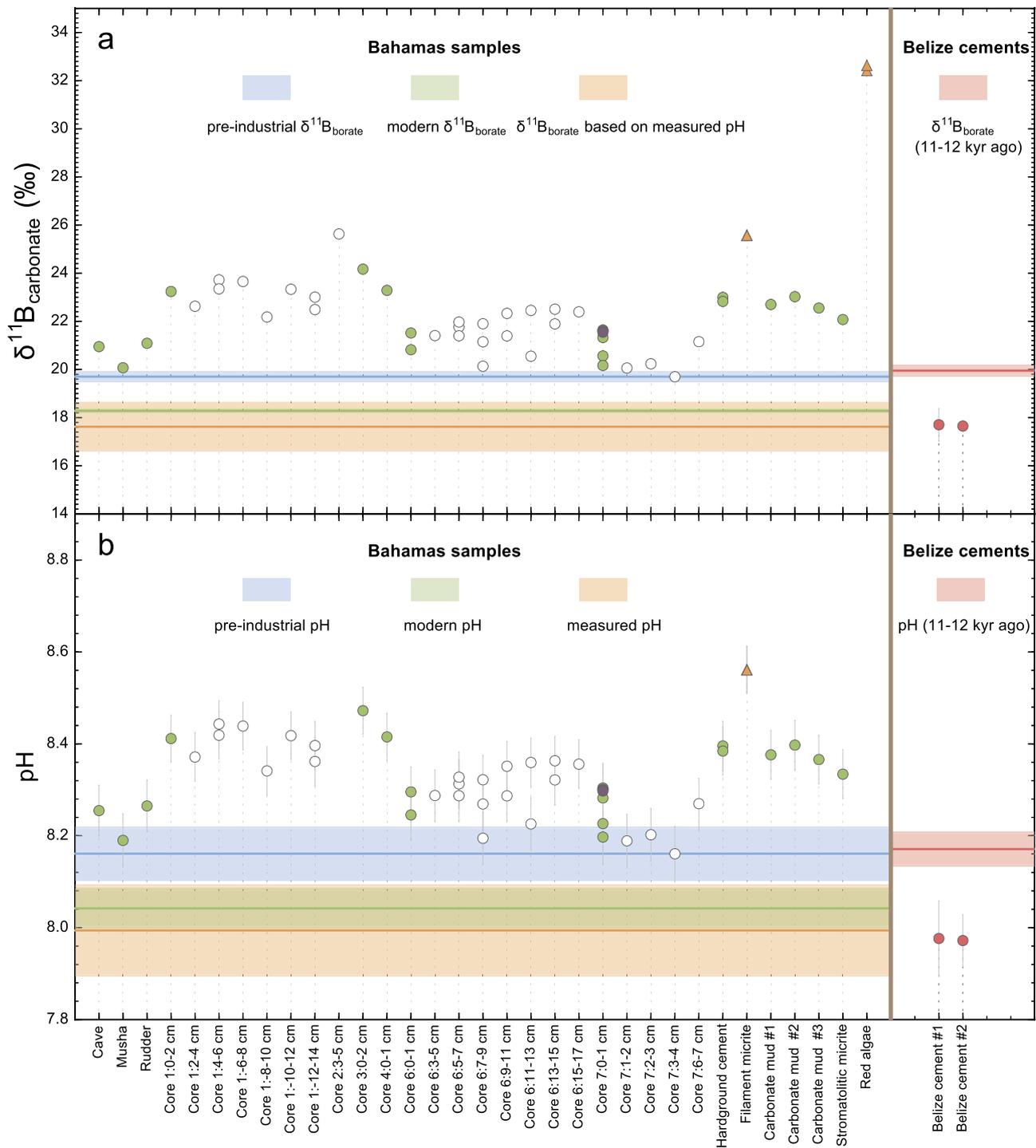
Fig. 3. Observed $\delta^{11}B_{carbonate}$ and back-calculated pH for carbonate samples. Filled green circles, purple circles and orange triangles represent core-top samples, while the white circles represent the down-core samples. Filled red circles denote Belize cements. For the same sample, multiple data points represent complete replicate analyses (i.e. samples re-picked, cleaned, and passed through columns). One exception is the purple circle, which represents the same sample (after dissolution) passed through columns on separate days and measured on separate days as described in the text. The other exceptions are the orange triangles, which represent the same sample (after dissolution and passing columns) that was diluted into different boron concentrations (see Table 1) and measured in the same day. (a) The blue line represents average pre-industrial Holocene seawater $\delta^{11}B_{borate}$ (with shaded bands representing 2σ of monthly variability) calculated from the Takahashi et al. (2009) grid point close to our studied area, as explained in the Supp. Text. The green line and shaded band represents modern seawater $\delta^{11}B_{borate}$ and intra annual variability from Takahashi et al. (2009), as above. The orange line represents average seawater $\delta^{11}B_{borate}$ over one day (with shaded bands representing 2σ of hourly variability) at the site off Little Darby Island. The red line represents estimated seawater $\delta^{11}B_{borate}$ at the site of Belize cement sampling 11–12 kyr ago, with the shaded area denoting 2σ bounds of uncertainty. The error bar for each data point represents 2σ analytical uncertainties (see Table 1). (b) The blue line represents average pre-industrial Holocene seawater pH (with shaded bands representing 2σ of monthly variability) calculated from the Takahashi et al. (2009) grid point close to our studied area, as explained in the text. The green line and shaded band represents modern seawater pH and intra annual variability from Takahashi et al. (2009), as above. The orange line represents average seawater pH (converted to total scale) observed via microelectrode over one day (with shaded bands representing 2σ of hourly variability) at the site off Little Darby Island, as described in the text. The red line represents estimated seawater pH at the site of Belize cement sampling 11–12 kyr ago, with the shaded area denoting 2σ bounds of uncertainty. Note that no pH estimates were carried out for Core 2: 3–5 cm and red algae. The error bar for each data point derives from 2σ uncertainty generated using Monte Carlo analysis. (For interpretation of the references to color in this figure legend, the reader is referred to the web version of this article.)
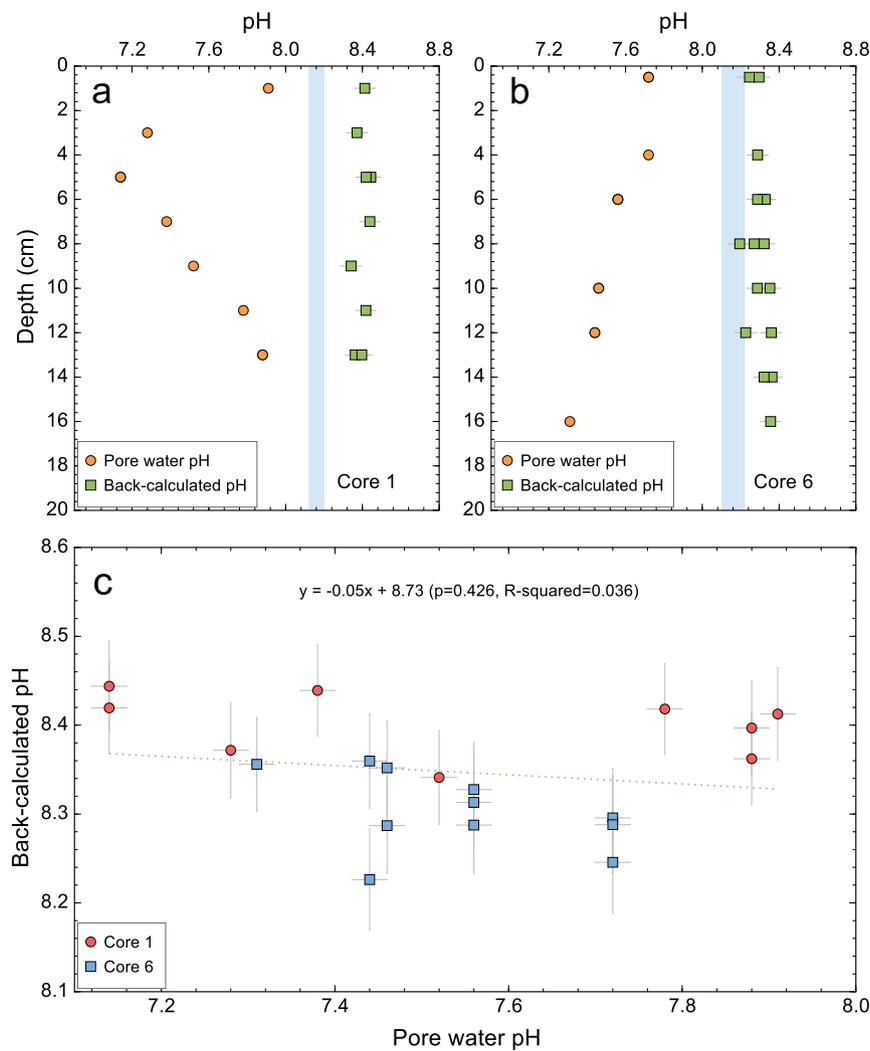
Fig. 4. Pore water pH, boron-derived pH and depth relationship. Pore water pH value and back-calculated pH values along Core 1 (Panel a) and Core 6 (Panel b). Note that pore water pH values are in NBS scale, which here is ∼0.14 higher than that in total pH scale (Van Heuven et al., 2011). The blue column represents the calculated pre-industrial Holocene pH range close to our studied area. As well as being uniformly higher than pore water pH (even if the pore water pH is in NBS scale), most back-calculated pH values are higher than pre-industrial pH estimates. Back-calculated pH values vs. pore water pH values are plotted in Panel c, with no significant relationship between the two variables (R-squared = 0.04, p = 0.43). Error bars for reconstructed pH represent 2σ. Error bars for pore water pH represent uncertainty in microelectrode pH measurements.

such a microenvironment. Sulfate reduction, an alternative driver of increased microenvironment carbonate saturation state, is less likely the dominant mechanism given the amount sulfate reduction needed to increase pH in an iron limited environment (e.g. Meister, 2013). Following ooid cortex formation, endolithic microbes (such as cyanobacteria; Reid and Macintyre, 2000) may have created the borings, some of which were subsequently filled by micritic cements (Fig. S1a, b). The activities of the boring microbes may have elevated the pH (e.g., through photosynthesis) in the microenvironment of the holes, again elevating $\delta^{11}B$ in the infillings relative to the $\delta^{11}B$ of borate ion in seawater. Different ooid grains display different boring intensities (Fig. S1a), suggesting heterogeneity in the extent of microbial alteration. The large $\delta^{11}B$ variability we observe may therefore in part arise from differing intensity of autotroph activity, as well as temporal variability in microenvironmental conditions (e.g. pH and alkalinity) during and immediately subsequent to ooid formation.

Variations in the composition of ooid nuclei (Fig. 2c) may have also contributed to the variability in ooid $\delta^{11}B$ values. As mentioned above, although nuclei are typically micritic, some nuclei consist of random grains (e.g. pellets, peloids and minor bioclasts). For the identifiable bioclasts (skeletal fragments), they represent less than 4% of grain nuclei. The majority of these bioclasts (if

any) are fragments of foraminifera (low-Mg calcite) based on thin section observations, in agreement with XRD measurements (the weight percent of low-Mg calcite ranges from 0 to 6.5%, with the majority close to 0%). No coral fragments are visible in thin sections. Since low-Mg foraminifera typically have a much lower boron concentration than aragonite, these minor bioclasts are not expected to exert a significant influence on the boron isotope ratios. However, in the case of the wholly micritized nuclei, or the micritized pellets or peloids in the nuclei, it is possible that varying contributions from high-Mg calcite (the second most abundant mineral in our ooids) may cause $\delta^{11}B$ values to vary. High-Mg calcite red algae is abundant in this area and it is conceivable that fragments from red algae could be micritized and contribute to the nuclei of our ooids. While there is little relationship (R-squared = 0.10, p = 0.06) between a sample's offset from $\delta^{11}B_{borate}$ and the wt.% high-Mg calcite from bulk XRD analysis, to further explore the possible influence of high-Mg calcite on $\delta^{11}B$ of ooids, we re-calculated the pH inferred by $\delta^{11}B$ using Eq. (1), accounting for varying contributions of high-Mg calcite. Two scenarios were tested. The first scenario assumed the high-Mg calcite component had the same boron isotope fractionation behavior as the inorganic calcite precipitates of Noireaux et al. (2015), with the same B/Ca ratio as aragonite (specifically, prescribed B/Ca = 265 μmol/mol,
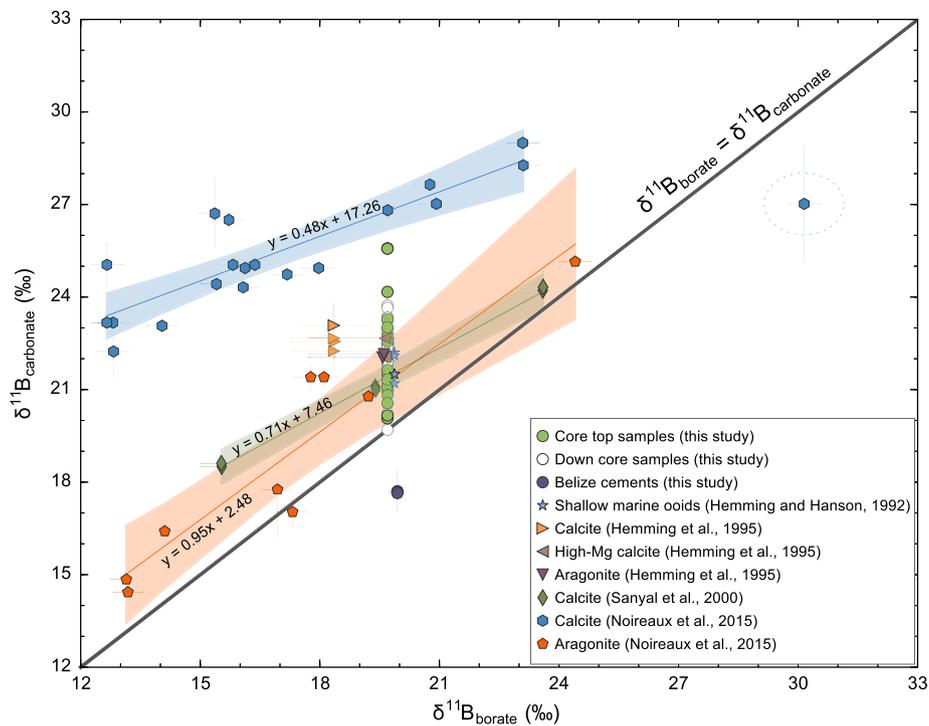
Fig. 5. The $\delta^{11}B$ of our shallow marine carbonates plotted with other published inorganic carbonates against the $\delta^{11}B$ of the borate ion in the solution assuming $^{11-10}K_B$ is 1.0272 ± 0.0006 (Klochko et al., 2006). All samples are normalized to modern $\delta^{11}B_{sw}$ (39.61‰; Foster et al., 2010) according to Zeebe and Wolf-Gladrow (2001), and pK_B^* was calculated for Mg-free seawater (Sanyal et al., 2000) according to the MyAMI model from Hain et al. (2015). For non-seawater solutions from Hemming et al. (1995), pK_B^* was calculated using a development version of MyAMI (Hain, pers. comm.). The error bar for each data point stands for 2σ. Also note that $\delta^{11}B_{carbonate}$ data of the Bahamas are plotted against the $\delta^{11}B_{borate}$ in seawater estimated for pre-industrial conditions. Shaded regions are 2σ bounds of uncertainty on each calibration line (the center line in the shaded area). The $\delta^{11}B$ of aragonite from Noireaux et al. (2015) is closest to the aqueous borate within the 2σ uncertainty while their $\delta^{11}B$ of calcite is above the 1:1 line and the pH sensitivity of $\delta^{11}B$ in calcite is lower than that of $\delta^{11}B$ in the borate ion. If plotted assuming $^{11-10}K_B$ is 1.026 ± 0.001 (Nir et al., 2015) in Fig. S2, then $\delta^{11}B$ of aragonite from Noireaux et al. (2015) is identical to the aqueous borate within the 2σ uncertainty. Note, following Noireaux et al. (2015), the plotted calibration for calcites excludes one high pH sample (circled).

$\delta^{11}B = 26.8‰$). The second scenario assumed all of the high-Mg calcite component derives from coralline algae, with the chemical composition of our measured red algae (B/Ca = 716 µmol/mol, $\delta^{11}B = 32.5‰$; see Table 1). Since [B] and $\delta^{11}B$ measured in our red algae were very high, this could be considered the extreme end-member scenario for the influence of high-Mg calcite on ooid $\delta^{11}B$. In the first case, the mass balance considerations bring estimated pH values closer to the pre-industrial pH ranges, but many data points are still out of the range of feasible ocean pH for this region (Fig. S3a). In the second case, many data points fall into the pre-industrial pH ranges and some even enter the modern pH field (Fig. S3b), indicating that contribution from red algal high-Mg calcite could account for some of the elevated $\delta^{11}B$ values in our ooids. However, in either case, the pH estimates still display a large variance among cores, along depth in the same core or even for the repeated samples from the same depth of the same core. Further, the second case, which assumes 100% of the high-Mg calcite is coralline algae, is unlikely as abiotic high-Mg calcite is also common in the region (e.g. Planavsky and Ginsburg, 2009). Thus, contamination from high-Mg calcite may partially explain the elevated $\delta^{11}B$ signal but is unlikely to be the only factor accounting for the deviation of boron-derived pH estimates from seawater pH values. Thus, we tentatively suggest that the observed range in boron isotope measurements in ooids and peloids reflects a combination of varying importance of microbial activity in mediating carbonate precipitation and subsequent alteration, with a possible effect from variable nuclei/core components.

An alternative scenario, whereby the variable $\delta^{11}B$ signals observed in our shallow marine carbonates are diagenetic in origin, is harder to reconcile with our measurements. Unlike in the Pliocene–Pleistocene Clino core from the Great Bahama Bank

(Stewart et al., 2015), the depositional setting of our samples argues against any influence of meteoric diagenesis in these carbonates (i.e. all cores excepting Core 1 are fully subtidal). Sub-aerial exposure is unlikely given that ooids are only up to several thousand years old and there are no dramatic sea level changes (e.g. from glaciation) during this time. Furthermore, meteoric diagenesis is expected to produce lower values of $\delta^{11}B$ (Stewart et al., 2015), whereas the majority of our data is elevated relative to seawater borate ion. Also, meteoric diagenesis should lower the $\delta^{13}C$, $\delta^{18}O$ and B/Ca of carbonates, but our samples have values within the normal range of unaltered shallow marine carbonates (Grammer et al., 1993; Swart et al., 2009). In fact, our measured $\delta^{18}O$ values (excepting that for high-Mg calcite red algae) display approximately equilibrium fractionation values from seawater (see Table S10). What's more, there is no correlation between $\delta^{11}B$ and either $\delta^{13}C$ (R-squared = 0.02, $p = 0.41$) or $\delta^{18}O$ (R-squared = 0.02, $p = 0.35$) for Bahamas ooids, which further suggests a lack of secondary meteoric diagenetic influence on these data. Diagenesis in pore water could also change the boron isotope signal in the ooids (through dissolution and re-precipitation of carbonates). However, there is no correlation between pore water pH values and the back calculated pH values (Fig. 4c). In addition, the pH of pore water in the presence of sea grass area is generally lower than that in bare oolitic sands at the same depth (in agreement with Burdige and Zimmerman, 2002). This could lead to a lower $\delta^{11}B$ signal in cores taken from below dense sea grass compared to those in the bare oolitic sands if carbonate is precipitating from these pore waters. However, this is not observed. Core 4 and Core 6 (dense sea grass overlying ooid sand) display higher $\delta^{11}B$ in carbonates than Core 7 (bare oolitic sand), arguing against early diagenesis as a dominant factor controlling boron isotope variation in our samples.

Microbial processes, by contrast, clearly drive some of the variation we observe. Cyanobacterial filament micrite (as relatively pure aragonite) provide an extreme example of microbal influence on carbonate precipitation, with a pH calculated from filament micrite of 8.56. This pH of 8.56 is the highest of all the samples, and can be readily attributed to photosynthetic CO_2 uptake by cyanobacteria, given that cyanobacteria are known to elevate extra-cellular pH sufficiently through photosynthesis to induce calcification (e.g. Bissett et al., 2008; Thompson and Ferris, 1990). In the case of hardground cements (as relatively pure aragonites), it is likely that the pH of these samples may be shifted, relative to overlying seawater, by similar microbial metabolic processes over relatively longer time periods. Dravis (1979) suggests that bacterial filaments are critical to cementation in the oolitic hardground environments of the Bahamas through binding of sediment and providing sites of cementation. Stromatolite lithification is also associated with microbial mats (Dupraz and Visscher, 2005; Reid et al., 2000; Stolz et al., 2009), in which cyanobacteria often play a significant role. Sulfate reduction has been commonly invoked as the key process in driving cementation in the Bahamian stromatolites (e.g. Dupraz and Visscher, 2005), and in Fe-poor carbonate sediments this should lower pH (e.g. Ben-Yaakov, 1973). Our observations that stromatolitic micrite record a higher pH value than seawater suggests that photosynthesis, rather than sulfate reduction, may instead be the dominant factor driving precipitation.

In contrast to the Bahamas samples, the pH inferred from δ^{11}B in Belize reef cements is lower than the seawater pH value estimated from this area. This is surprising, since these cements are thought to precipitate from seawater of normal salinity and major ion chemistry at moderate marine depths (Ginsburg and James, 1976). However, it is possible that the pH of semi-restricted reef cavities where these cements precipitate may be lower relative to surrounding seawater pH. Decomposition of organic matter within the reef framework can result in the consumption of oxygen, an increase in alkalinity, and lowering of pH in pore fluids (e.g. Sansone et al., 1988). Therefore, δ^{11}B of these marine cements could be reasonably predicted to be lower than the seawater borate value. However, this explanation would need to be reconciled with carbon isotope profiles in Belize cements that are quite positive ($+4\permil$ to $+5\permil$) and fall well within the field for isotopically-enriched marine cements precipitated from normal seawater (Ginsburg and James, 1976; Grammer et al., 1993).

4.3. Implications for δ^{11}B records from shallow marine carbonates

Unfortunately, the elevated and variable δ^{11}B signals of carbonates from this study cast doubt on the utility of these types of shallow marine non-skeletal carbonates (ooids, peloids, cements, calcified filaments, and micritic sediments) as straightforward seawater pH archives without first carefully considering the complex provenance of the carbonates analyzed. Here, we hypothesize that similar issues might exist for shallow water carbonates in deep time. Micritic sediments (or technically the recrystallized product of fine grained carbonates) have been the focus of many 'deep time' B isotope studies (e.g. Clarkson et al., 2015; Ohnemueller et al., 2014). While it is not yet possible to make any broad conclusions on the basis of our limited micritic sediment analyses, even in the modern Bahamas, micrite has numerous origins (e.g., from green algae, micritized bioclasts, calcified cyanobacteria) (e.g. Broecker et al., 2000; Gischler et al., 2013; Reid et al., 1992; Robbins et al., 1997). It has also been suggested that similar biologically-derived carbonates are a primary component of some deep time low-Mg micrite (Pratt, 2001). Therefore, in the light of the variable and predominantly physiologically-derived pH signals we observe here, we encourage further efforts to better establish the relative importance of environmental and biological

factors in determining δ^{11}B in non-skeletal shallow marine carbonates.

5. Conclusions

Ooids, peloids, hardground cements, calcified filament micrite, carbonate mud and stromatolitic micrite from the Bahamas and botryoidal cements from the Belize barrier reef complex were collected to test the potential of applying the boron isotope-pH proxy to inorganic shallow marine carbonates. For the Bahamas, the pH values inferred from our core samples are scattered (8.16–8.56) and are generally higher than estimated modern or pre-industrial pH at these sites, with elevation not consistent across all samples. The δ^{11}B and hence back-calculated pH shows no correlation with pore water pH values, nor any systematic variation with core depth, and also differ between nearby cores. By contrast, pH estimates ($\sim$7.98) for Belize reef cements are lower than likely seawater pH ($\sim$8.17) at the time of formation. We suggest the variation of δ^{11}B in these non-skeletal carbonates relative to ambient borate is unlikely to be explained by meteoric or pore water diagenesis, and, in the case of ooids and peloids, it cannot be completely explained by varying nuclei components. Instead, we suggest that offsets may derive from microbially-mediated carbonate precipitation and/or alteration. From the perspective of palaeo-pH reconstruction, variability between nearby cores and across different carbonate substrates highlights the importance of duplicating palaeo-records from multiple settings. Widespread non-equilibrium values of δ^{11}B emphasize the need for further investigation of the determinants of δ^{11}B in modern marine non-skeletal carbonates before they can be used to estimate seawater pH in the fossil record. In this regard, more spatially-resolved analytical techniques, such as laser ablation, may be valuable. More positively, this study provides new and independent evidence for the microbial mediation of shallow marine carbonate formation. Specifically, the elevated δ^{11}B signal in our carbonates strongly implicates CO_2 uptake by microbial photosynthesis in driving the precipitation of carbonates, rather than sulfate reduction, which would more likely lower ambient pH.

Appendix A. Supplementary material

Supplementary material related to this article can be found online at http://dx.doi.org/10.1016/j.epsl.2016.10.059.

References

Anagnostou, E., John, E.H., Edgar, K.M., Foster, G.L., Ridgwell, A., Inglis, G.N., Pancost, R.D., Lunt, D.J., Pearson, P.N., 2016. Changing atmospheric CO_2 concentration was the primary driver of early Cenozoic climate. Nature 533, 380–384. http://dx.doi.org/10.1038/nature17423.

Ben-Yaakov, S., 1973. pH buffering of pore water of recent anoxic marine sediments. Limnol. Oceanogr. 18, 86–94. http://dx.doi.org/10.4319/lo.1973.18.1.0086.

Berkyová, S., Munnecke, A., 2010. "Calcispheres" as a source of lime mud and peloids–evidence from the early Middle Devonian of the Prague Basin, The Czech Republic. Bull. Geosci. 85.

Bissett, A., Reimer, A., de Beer, D., Shiraishi, F., Arp, G., 2008. Metabolic microenvironmental control by photosynthetic biofilms under changing macroenvironmental temperature and pH conditions. Appl. Environ. Microbiol. 74, 6306–6312. http://dx.doi.org/10.1128/AEM.00877-08.

Broecker, W.S., Sanyal, A., Takahashi, T., 2000. The origin of Bahamian Whitings revisited. Geophys. Res. Lett. 27, 3759–3760. http://dx.doi.org/10.1029/2000GL011872.

Burdige, D.J., Zimmerman, R.C., 2002. Impact of sea grass density on carbonate dissolution in Bahamian sediments. Limnol. Oceanogr. 47, 1751–1763.

Clarkson, M.O., Kasemann, S.A., Wood, R.A., Lenton, T.M., Daines, S.J., Richoz, S., Ohnemueller, F., Meixner, A., Poulton, S.W., Tipper, E.T., 2015. Ocean acidification and the Permo-Triassic mass extinction. Science 348, 229–232. http://dx.doi.org/10.1126/science.aaa0193.

Davies, P.J., Bubela, B., Ferguson, J., 1978. The formation of ooids. Sedimentology 25, 703–730. http://dx.doi.org/10.1111/j.1365-3091.1978.tb00326.x.

Diaz, M.R., Piggot, A.M., Eberli, G.P., Klaus, J.S., 2013. Bacterial community of oolitic carbonate sediments of the Bahamas Archipelago. Mar. Ecol. Prog. Ser. 485, 9–24. http://dx.doi.org/10.3354/meps10359.

Dravis, J., 1979. Rapid and widespread generation of Recent oolitic hardgrounds on a high energy Bahamian platform, Eleuthera Bank, Bahamas. J. Sediment. Res. 49, 195–207. http://dx.doi.org/10.1306/212F76EE-2B24-11D7-8648000102C1865D.

Duguid, S.M.A., Kyser, T.K., James, N.P., Rankey, E.C., 2010. Microbes and ooids. J. Sediment. Res. 80, 236–251. http://dx.doi.org/10.2110/jsr.2010.027.

Dupraz, C., Visscher, P.T., 2005. Microbial lithification in marine stromatolites and hypersaline mats. Trends Microbiol. 13, 429–438. http://dx.doi.org/10.1016/j.tim.2005.07.008.

Foster, G.L., 2008. Seawater pH, pCO₂ and [CO₃²⁻] variations in the Caribbean Sea over the last 130 kyr: a boron isotope and B/Ca study of planktic foraminifera. Earth Planet. Sci. Lett. 271, 254–266. http://dx.doi.org/10.1016/j.epsl.2008.04.015.

Foster, G.L., Pogge von Strandmann, P.A.E., Rae, J.W.B., 2010. Boron and magnesium isotopic composition of seawater. Geochem. Geophys. Geosyst. 11, Q08015. http://dx.doi.org/10.1029/2010GC003201.

Ginsburg, R.N., James, N.P., 1976. Submarine botryoidal aragonite in Holocene reef limestones, Belize. Geology 4, 431–436. http://dx.doi.org/10.1130/0091-7613(1976)4<431:SBAIHR>2.0.CO;2.

Ginsburg, R.N., Planavsky, N.J., 2008. Diversity of Bahamian microbialite substrates. In: Dilek, Y., Furnes, H., Muehlenbachs, K. (Eds.), Links Between Geological Processes, Microbial Activities & Evolution of Life. In: Modern Approaches in Solid Earth Sciences. Springer, Netherlands, pp. 177–195.

Gischler, E., Dietrich, S., Harris, D., Webster, J.M., Ginsburg, R.N., 2013. A comparative study of modern carbonate mud in reefs and carbonate platforms: mostly biogenic, some precipitated. Sediment. Geol. 292, 36–55. http://dx.doi.org/10.1016/j.sedgeo.2013.04.003.

Grammer, G.M., Ginsburg, R.N., Swart, P.K., McNeill, D.F., Jull, A.J.T., Prezbindowski, D.R., 1993. Rapid growth rates of syndepositional marine aragonite cements in steep marginal slope deposits, Bahamas and Belize. J. Sediment. Res. 63, 983–989. http://dx.doi.org/10.1306/D4267C62-2B26-11D7-8648000102C1865D.

Hain, M.P., Sigman, D.M., Higgins, J.A., Haug, G.H., 2015. The effects of secular calcium and magnesium concentration changes on the thermodynamics of seawater acid/base chemistry: implications for Eocene and Cretaceous ocean carbon chemistry and buffering. Glob. Biogeochem. Cycles 29. http://dx.doi.org/10.1002/2014GB004986. 2014GB004986.

Hemming, N.G., Hanson, G.N., 1992. Boron isotopic composition and concentration in modern marine carbonates. Geochim. Cosmochim. Acta 56, 537–543. http://dx.doi.org/10.1016/0016-7037(92)90151-8.

Hemming, N.G., Reeder, R.J., Hanson, G.N., 1995. Mineral–fluid partitioning and isotopic fractionation of boron in synthetic calcium carbonate. Geochim. Cosmochim. Acta 59, 371–379. http://dx.doi.org/10.1016/0016-7037(95)00288-B.

Henehan, M.J., Rae, J.W.B., Foster, G.L., Erez, J., Prentice, K.C., Kucera, M., Bostock, H.C., Martínez-Botí, M.A., Milton, J.A., Wilson, P.A., Marshall, B.J., Elliott, T., 2013. Calibration of the boron isotope proxy in the planktonic foraminifera Globigerinoides ruber for use in palaeo-CO₂ reconstruction. Earth Planet. Sci. Lett. 364, 111–122. http://dx.doi.org/10.1016/j.epsl.2012.12.029.

Hönisch, B., Hemming, N.G., Archer, D., Siddall, M., McManus, J.F., 2009. Atmospheric carbon dioxide concentration across the mid-Pleistocene transition. Science 324, 1551–1554. http://dx.doi.org/10.1126/science.1171477.

Hu, X., Burdige, D.J., 2007. Enriched stable carbon isotopes in the pore waters of carbonate sediments dominated by seagrasses: evidence for coupled carbonate dissolution and reprecipitation. Geochim. Cosmochim. Acta 71, 129–144. http://dx.doi.org/10.1016/j.gca.2006.08.043.

Kazmierczak, J., Coleman, M.L., Gruszczynski, M., Kempe, S., 1996. Cyanobacterial key to the genesis of micritic and peloidal limestones in ancient seas. Acta Palaeontol. Pol. 4, 319–338.

Kiss, E., 1988. Ion-exchange separation and spectrophotometric determination of boron in geological materials. Anal. Chim. Acta 211, 243–256. http://dx.doi.org/10.1016/S0003-2670(00)83684-3.

Klochko, K., Kaufman, A.J., Yao, W., Byrne, R.H., Tossell, J.A., 2006. Experimental measurement of boron isotope fractionation in seawater. Earth Planet. Sci. Lett. 248, 276–285. http://dx.doi.org/10.1016/j.epsl.2006.05.034.

Land, L.S., Behrens, E.W., Frishman, S.A., 1979. The ooids of Baffin Bay, Texas. J. Sediment. Res. 49, 1269–1277. http://dx.doi.org/10.1306/212F7905-2B24-11D7-8648000102C1865D.

Lowenstam, H.A., Epstein, S., 1957. On the origin of sedimentary aragonite needles of the Great Bahama Bank. J. Geol. 65, 364–375.

Macintyre, I.G., Reid, R.P., 1995. Crystal alteration in a living calcareous alga (Halimeda); implications for studies in skeletal diagenesis. J. Sediment. Res. 65, 143–153. http://dx.doi.org/10.1306/D4268054-2B26-11D7-8648000102C1865D.

Meister, P., 2013. Two opposing effects of sulfate reduction on carbonate precipitation in normal marine, hypersaline, and alkaline environments. Geology 41, 499–502. http://dx.doi.org/10.1130/G34185.1.

Morse, J.W., Mackenzie, F.T., 1990. Geochemistry of Sedimentary Carbonates, vol. 48, 1 edition. Elsevier Science, Amsterdam, New York NY, U.S.A.

Morse, J.W., Zullig, J.J., Bernstein, L.D., Millero, F.J., Milne, P.J., Mucci, A., Choppin, G.R., 1985. Chemistry of calcium carbonate-rich shallow water sediments in the Bahamas. Am. J. Sci. 285, 147–185. http://dx.doi.org/10.2475/ajs.285.2.147.

Nir, O., Vengosh, A., Harkness, J.S., Dwyer, G.S., Lahav, O., 2015. Direct measurement of the boron isotope fractionation factor: reducing the uncertainty in reconstructing ocean paleo-pH. Earth Planet. Sci. Lett. 414, 1–5. http://dx.doi.org/10.1016/j.epsl.2015.01.006.

Noireaux, J., Mavromatis, V., Gaillardet, J., Schott, J., Montouillout, V., Louvat, P., Rollion-Bard, C., Neuville, D.R., 2015. Crystallographic control on the boron isotope paleo-pH proxy. Earth Planet. Sci. Lett. 430, 398–407. http://dx.doi.org/10.1016/j.epsl.2015.07.063.

Ohnemueller, F., Prave, A.R., Fallick, A.E., Kasemann, S.A., 2014. Ocean acidification in the aftermath of the Marinoan glaciation. Geology 42, 1103–1106. http://dx.doi.org/10.1130/G35937.1.

Okai, T., Suzuki, A., Kawahata, H., Terashima, S., Imai, N., 2002. Preparation of a new geological survey of Japan geochemical reference material: coral JCp-1. Geostand. Newsl. 26, 95–99. http://dx.doi.org/10.1111/j.1751-908X.2002.tb00627.x.

Planavsky, N., Ginsburg, R.N., 2009. Taphonomy of modern marine Bahamian microbialites. Palaios 24, 5–17. http://dx.doi.org/10.2110/palo.2008.p08-001r.

Planavsky, N., Reid, R.P., Lyons, T.W., Myshrall, K.L., Visscher, P.T., 2009. Formation and diagenesis of modern marine calcified cyanobacteria. Geobiology 7, 566–576. http://dx.doi.org/10.1111/j.1472-4669.2009.00216.x.

Pratt, B.R., 2001. Calcification of cyanobacterial filaments: Girvanella and the origin of lower Paleozoic lime mud. Geology 29, 763–766. http://dx.doi.org/10.1130/0091-7613(2001)029<0763:COCFGA>2.0.CO;2.

Rae, J.W.B., Foster, G.L., Schmidt, D.N., Elliott, T., 2011. Boron isotopes and B/Ca in benthic foraminifera: proxies for the deep ocean carbonate system. Earth Planet. Sci. Lett. 302, 403–413. http://dx.doi.org/10.1016/j.epsl.2010.12.034.

Reid, R.P., Macintyre, I.G., 1998. Carbonate recrystallization in shallow marine environments: a widespread diagenetic process forming micritized grains. J. Sediment. Res. 68, 928–946. http://dx.doi.org/10.2110/jsr.68.928.

Reid, R.P., Macintyre, I.G., 2000. Microboring versus recrystallization: further insight into the micritization process. J. Sediment. Res. 70, 24–28. http://dx.doi.org/10.1306/2DC408FA-0E47-11D7-8643000102C1865D.

Reid, R.P., Macintyre, I.G., Post, J.E., 1992. Micritized skeletal grains in northern Belize Lagoon; a major source of Mg-calcite mud. J. Sediment. Res. 62, 145–156. http://dx.doi.org/10.1306/D42678B1-2B26-11D7-8648000102C1865D.

Reid, R.P., Visscher, P.T., Decho, A.W., Stolz, J.F., Bebout, B.M., Dupraz, C., Macintyre, I.G., Paerl, H.W., Pinckney, J.L., Prufert-Bebout, L., Steppe, T.F., DesMarais, D.J., 2000. The role of microbes in accretion, lamination and early lithification of modern marine stromatolites. Nature 406, 989–992. http://dx.doi.org/10.1038/35023158.

Robbins, L.L., Tao, Y., Evans, C.A., 1997. Temporal and spatial distribution of whitings on Great Bahama Bank and a new lime mud budget. Geology 25, 947–950. http://dx.doi.org/10.1130/0091-7613(1997)025<0947:TASDOW>2.3.CO;2.

Romaniello, S.J., Herrmann, A.D., Anbar, A.D., 2013. Uranium concentrations and ²³⁸U/²³⁵U isotope ratios in modern carbonates from the Bahamas: assessing a novel paleoredox proxy. In: Special Issue dedicated to H.D. Holland: Evolution of the atmosphere and ocean through time. Chem. Geol. 362, 305–316. http://dx.doi.org/10.1016/j.chemgeo.2013.10.002.

Sansone, F.J., Andrews, C.C., Buddemeier, R.W., Tribble, G.W., 1988. Well-point sampling of reef interstitial water. Coral Reefs 7, 19–22. http://dx.doi.org/10.1007/BF00301977.

Sanyal, A., Nugent, M., Reeder, R.J., Bijma, J., 2000. Seawater pH control on the boron isotopic composition of calcite: evidence from inorganic calcite precipitation experiments. Geochim. Cosmochim. Acta 64, 1551–1555. http://dx.doi.org/10.1016/S0016-7037(99)00437-8.

Stewart, J.A., Gutjahr, M., Pearce, F., Swart, P.K., Foster, G.L., 2015. Boron during meteoric diagenesis and its potential implications for Marinoan snowball Earth δ¹¹B-pH excursions. Geology 43, 627–630. http://dx.doi.org/10.1130/G36652.1.

Stolz, J.F., Reid, R.P., Visscher, P.T., Decho, A.W., Norman, R.S., Aspden, R.J., Bowlin, E.M., Franks, J., Foster, J.S., Paterson, D.M., Przekop, K.M., Underwood, G.J.C.,

Prufert-Bebout, L., 2009. The microbial communities of the modern marine stromatolites at Highborne Cay, Bahamas. Atoll Res. Bull., 1–29. http://dx.doi.org/10.5479/si.00775630.567.1.

Summons, R.E., Bird, L.R., Gillespie, A.L., Pruss, S.B., Roberts, M., Sessions, A.L., 2013. Lipid biomarkers in ooids from different locations and ages: evidence for a common bacterial flora. Geobiology 11, 420–436. http://dx.doi.org/10.1111/gbi.12047.

Swart, P.K., James, N.P., Mallinson, D., Malone, M.J., Matsuda, H., Simo, T., 2002. 10. Data report: carbonate mineralogy of sites drilled during Leg 182.

Swart, P.K., Reijmer, J.J., Otto, R., 2009. A Re-evaluation of facies on Great Bahama Bank II: variations in the δ^{13}C, δ^{18}O and mineralogy of surface sediments. In: Perspect. Carbonate Geol.: Tribute to the Career of Robert Nathan Ginsburg, pp. 47–59.

Takahashi, T., Sutherland, S.C., Wanninkhof, R., Sweeney, C., Feely, R.A., Chipman, D.W., Hales, B., Friederich, G., Chavez, F., Sabine, C., Watson, A., Bakker, D.C.E., Schuster, U., Metzl, N., Yoshikawa-Inoue, H., Ishii, M., Midorikawa, T., Nojiri, Y., Körtzinger, A., Steinhoff, T., Hoppema, M., Olafsson, J., Arnarson, T.S., Tilbrook, B., Johannessen, T., Olsen, A., Bellerby, R., Wong, C.S., Delille, B., Bates, N.R., de Baar, H.J.W., 2009. Climatological mean and decadal change in surface ocean pCO$_2$, and net sea–air CO$_2$ flux over the global oceans. Deep Sea Res. Part II 56, 554–577. http://dx.doi.org/10.1016/j.dsr2.2008.12.009. Top Stud. Oceanogr., Surface Ocean CO$_2$ Variability and Vulnerabilities.

Thompson, J.B., Ferris, F.G., 1990. Cyanobacterial precipitation of gypsum, calcite, and magnesite from natural alkaline lake water. Geology 18, 995–998. http://dx.doi.org/10.1130/0091-7613(1990)018<0995:CPOGCA>2.3.CO;2.

Van Heuven, S., Pierrot, D., Rae, J.W.B., Lewis, E., Wallace, D.W.R., 2011. MATLAB program developed for CO$_2$ system calculations. ORNLCDIAC-105b. Carbon Dioxide Inf. Anal. Cent. Oak Ridge Natl. Lab., US Dep. Energy, Oak Ridge, Tenn.

Vogl, J., Rosner, M., 2012. Production and certification of a unique set of isotope and delta reference materials for boron isotope determination in geochemical, environmental and industrial materials. Geostand. Geoanal. Res. 36, 161–175. http://dx.doi.org/10.1111/j.1751-908X.2011.00136.x.

Zeebe, R.E., Wolf-Gladrow, D., 2001. CO$_2$ in Seawater: Equilibrium, Kinetics, Isotopes, vol. 65, 1 edition. Elsevier Science, Amsterdam, New York.